2012

In Situ and Ex Situ Studies of Molybdenum Thin Films Deposited by rf and dc Magnetron Sputtering as a Back Contact for CIGS Solar Cells

K. P. Aryal
Old Dominion University, karya001@odu.edu

H. Khatri

R. W. Collins

S. Marsillac
Old Dominion University, Smarsill@odu.edu

Original Publication Citation

Aryal, K., Khatri, H., Collins, R.W., & Marsillac, S. (2012). In situ and ex situ studies of molybdenum thin films deposited by rf and dc magnetron sputtering as a back contact for CIGS solar cells. *International Journal of Photoenergy*. doi: 10.1155/2012/723714

Hindawi Publishing Corporation
International Journal of Photoenergy
Volume 2012, Article ID 723714, 7 pages
doi:10.1155/2012/723714

Research Article

In Situ and *Ex Situ* Studies of Molybdenum Thin Films Deposited by rf and dc Magnetron Sputtering as a Back Contact for CIGS Solar Cells

K. Aryal,[1] H. Khatri,[2] R. W. Collins,[2] and S. Marsillac[1]

[1] *Department of Electrical and Computer Engineering, Old Dominion University, Norfolk, VA 23529, USA*
[2] *Wright Center for Photovoltaic Innovation and Commercialization, University of Toledo, Toledo, OH 43606, USA*

Correspondence should be addressed to S. Marsillac, smarsill@odu.edu

Received 16 December 2011; Accepted 31 January 2012

Academic Editor: Bhushan Sopori

Molybdenum thin films were deposited by rf and dc magnetron sputtering and their properties analyzed with regards to their potential application as a back contact for CIGS solar cells. It is shown that both types of films tend to transition from tensile to compressive strain when the deposition pressure increases, while the conductivity and the grain size decreas. The nucleation of the films characterized by *in situ* and real time spectroscopic ellipsometry shows that both films follow a Volmer-Weber growth, with a higher surface roughness and lower deposition rate for the rf deposited films. The electronic relaxation time was then extracted as a function of bulk layer thickness for rf and dc films by fitting each dielectric function to a Drude free-electron model combined with a broad Lorentz oscillator. The values were fitted to a conical growth mode and demonstrated that the rf-deposited films have already smaller grains than the dc films when the bulk layer thickness is 30 nm.

1. Introduction

With 20.3% efficiency, $Cu(In,Ga)Se_2$ (CIGS) solar cells are the most efficient polycrystalline thin films solar cells today [1]. Part of the success of this technology comes from the underlying molybdenum layer. It fulfills most requirements for an effective back contact, notably chemical and mechanical compatibility with the other deposition processes, high conductivity, low contact resistance with the CIGS layer, and commensurate thermal expansion coefficient [2]. The deposition of a molybdenum film as a back contact is not by itself, however, an assurance of a high efficiency solar cell. The deposition process and parameters play a key role in obtaining a layer with the appropriate properties. Extensive research has been done on the deposition of molybdenum thin films by direct-current (dc) sputtering [2–6]. As the potential portfolio of CIGS applications expand, different Mo film properties may be required to adapt to new requirements. In this paper, therefore, we have described the use of dc magnetron sputtering to deposit Mo thin films on soda-lime glass and the comparison of such films with those deposited by radio frequency (rf) magnetron sputtering. To our knowledge, much less research has been performed on Mo thin films deposited by this latter method [7–16]. To assess the potential of this process, the physical, electrical, and optical properties of rf and dc sputtered films were studied as a function of argon pressure via *ex situ* and *in situ* measurements.

2. Experimental Details

Molybdenum thin films were fabricated using rf and dc magnetron sputtering onto soda-lime glass (SLG) substrates. The deposition was carried out in high purity (99.999%) argon ambient using a 2 inch diameter Mo sputtering target. The argon flow was metered with a mass flow controller and fixed at 10 sccm. The required argon pressure for sputtering was achieved by throttling a high vacuum gate valve. The thickness for all depositions was kept constant at 0.7 μm. There was no intentional heating, but it should be noted that the substrate temperature increased to 310 K during the rf depositions. Uniform film thickness ($\pm$5% error)

was achieved using a rotatable substrate holder fixed 6 cm from the target. The argon pressure was varied between 4 and 20 mTorr while keeping a constant sputtering power of 100 W.

The structural, physical, electrical and optical properties of the films were studied as a function of deposition argon pressure. The influence of pressure on the crystallographic properties and the mechanical properties of the films were studied by X-ray diffraction (XRD) using a XPERT-PRO diffractometer. The X-ray scans were performed using CuK_α radiation ($\lambda_{CuK\alpha} = 0.154$ nm) in a scanning 2θ mode with 0.01° step size over a 2θ range of 20° to 90°. The adhesion of the films to the substrates was examined using an adhesive tape test. The samples were mechanically scribed to a rectangular shape, adhesive tape strips of the same length were attached to the scribed films, and the tape was stripped with approximately equal amounts of force. Failure of the test is evidence by any film's residue on the tape. The film resistivity was calculated from the sheet resistance by four-point probe and the film thickness by DekTak^{3}ST Surface Profiler. An atomic force microscope (AFM) operated in noncontact AC mode (320 KHz tip) was used for the topographical images of the films. The acquired AFM images were used to determine the root-mean square roughness (rms) of the films. Spectroscopic ellipsometry measurements were performed *in situ* with a rotating-compensator multichannel instrument in the energy range of 0.75 to 6.5 eV. In ellipsometry, two quantities, ψ and Δ, are measured in reflection; these represent, respectively, the relative amplitude ratio and the phase difference shift between the parallel and perpendicular field components as measured with respect to the plane of incidence in the reflection of polarized light. Pairs of (ψ, Δ) spectra were collected within a time of 1.5 sec. Analyses of the spectra involved numerical inversion and least-squares regression algorithms. The angle of incidence was at 65° [17, 18].

3. Results and Discussion

3.1. Physical Properties. The influence of pressure and deposition process on the crystallographic properties and the mechanical properties of the films was studied by XRD. As shown in Figure 1 (for $p = 10$ mTorr), the rf films tend to have a lower degree of crystallization compared to the dc films, as indicated by their broader and smaller peaks. It was also found that the films deposited with lower pressure had a higher degree of crystallinity as shown in Figure 2. This can be explained by the fact that at lower deposition pressures adatoms have impacted the surface with sufficient energy to enhance their mobility, leading to increased diffusion of atoms, atomic rearrangements, and atomic displacements, which in turn are conducive to the growth of more stable, larger crystalline grains. In the case of the rf films, since a longer deposition is required to achieve the same thickness, there may be an additional reduction of the mobility due to the introduction of contaminant species such as oxygen, which suppresses the diffusion of Mo adatoms and lead to lattice defects.

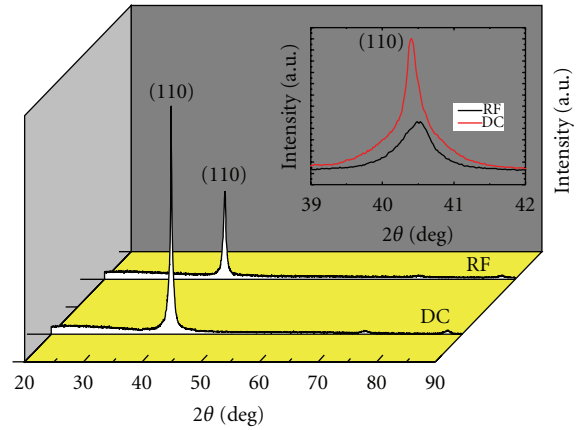

Figure 1: Typical XRD spectra of dc and rf magnetron sputtered molybdenum thin films at 10 mTorr. (Inset: closeup of the (110) peak).

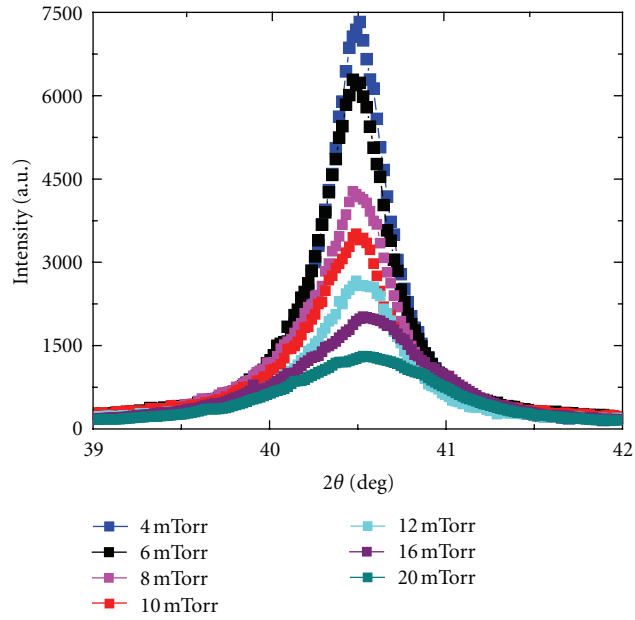

Figure 2: XRD pattern of the (110) peak for rf sputtered molybdenum thin film as a function of argon pressure.

The observed (110) peak distortion can be directly related to the strain in the films, which can be either compressive or tensile. The Bragg law was used to calculate the lattice spacing, $d_{(110)}$, and hence the lattice parameter a. The strain of the film was then calculated using the formula:

$$\text{Strain}(\%) = \frac{\Delta a}{a} \times 100, \tag{1}$$

where Δa is the change in lattice parameter in the film compared to a Mo sheet.

The change in strain with pressure for rf and dc films is shown in Figure 3. In both cases the tensile strain dominates

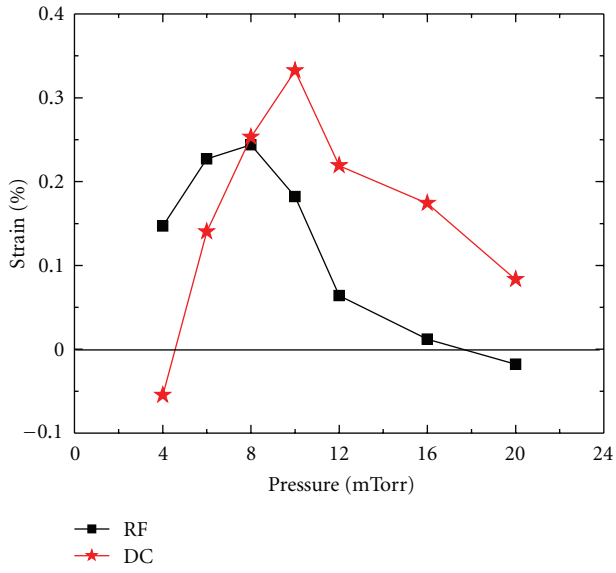

Figure 3: Strain variation in rf and dc films as a function of pressure; (the curves are a guide to the eye).

over compressive strain. These strain versus pressure curves can be split into low and high pressure domains. At low pressure, the films are under either low tensile or compressive strain. With increasing pressure, the tensile strain increases until it reaches a maximum. For the rf films, the maximum is about 0.24% at 8 mTorr, whereas for the dc films it is 0.33% at 10 mTorr. At high pressure, the tensile strain gradually decreases with further increasing pressure, leading toward or reaching compressive strain once again at pressures higher than 16 mTorr. The observed compressive strain at low pressures can be explained by an effect called "atomic peening" in which the high momentum sputtered ions impinge onto the growing film surface [19, 20]. In striking the surface with high momentum, the incident atoms drive the near-surface atoms of the film closer together. As a result, both incident and impacted atoms become embedded deeper into the film surface thus generating the film's compressive stress and concomitantly a denser film microstructure.

Conversely, the absence of energetic particle bombardment at high pressure leads to a tensile stress and to a more porous film microstructure. The compressive stress at the higher pressures is most probably influenced by lattice distortion due to one of the following: (i) incorporation of foreign atoms into the film, (ii) reaction at grain boundaries that produce a phase with a different molar volume, or (iii) surface energy reduction at void surfaces. It is important to notice that the nature and degree of the strain in the Mo films can potentially alter the chemical activity of selenium during the formation of the CIGS layer.

To assess the effect of strain, we measured the adhesion of the films on the substrate by using an adhesive tape test as described in Section 2. We found that all rf and dc films passed the test except for the dc films prepared at 4 mTorr. The failure of the test of the dc films at this pressure may be due to high compressive strain in the films, as observed in Figure 3.

The degree of orientation of the films along the (110) direction, $P(110)$, was calculated using:

$$P(110) = \frac{I(110)/I_0(110) + I(220)/I_0(220)}{\sum_{hkl} I(hkl)/I_0(hkl)}, \quad (2)$$

where $I(hkl)$ is the measured intensity of the (hkl) peak and $I_0(hkl)$ is the relative molybdenum powder diffraction intensity. The rf films did not show any correlation of $P(110)$ with pressure ($P(110) \sim 0.8$-0.9); however, $P(110)$ for the dc films was observed to decrease linearly from 0.96 to 0.87 for films of increasing pressure from 4 to 20 mTorr. The fact that the crystallites have a strong preferential orientation along the (110) plane can be explained by the lowest surface potential energy for these planes.

The variation of the full width at half maximum (FWHM) of the (110) peak with pressure for rf and dc films was also measured. The average grain size of the films was then determined using Scherrer formula [21]:

$$L = \frac{K\lambda}{\beta \cos(\theta)}, \quad (3)$$

where L is the crystallite size, K is the Scherrer constant (considered 0.90 for spherical particles), λ is the X-ray wavelength, β is the FWHM of the peak, corrected for instrument broadening (i.e., $\beta^2 = B^2 - b^2$ where B = experimental, b = instrumental), and θ is the Bragg angle. For both type of films, a decrease in grain size with increasing sputtering pressure was observed, followed by saturation above 12 mTorr (Figure 4). For all pressures, the dc films tend to have larger grain size than the rf films, which may be related to the higher deposition rate of the dc films and therefore the potential for lower foreign atom incorporation.

Film morphology measured by atomic force microscopy (AFM) is shown Figures 5(a) and 5(b) for 4 mTorr. The dc films show relatively smooth surface with uniform grain distribution, whereas the rf films have a wider range of grain sizes, a fibrous or columnar morphology and rougher surfaces. The rms roughness of the dc and rf films were found to increase from 2 nm to 6 nm and from 3 nm to 9 nm, respectively, as pressure increased from 4 mTorr to 20 mTorr. Furthermore, the films deposited at high sputtering pressures showed dendritic-like morphologies, and thus may incorporate high void volume fraction in the films. With an increasing concentration of small void structures with increasing pressure, the film volume may expand slightly into the void regions, leading to tensile stress. As the voids increase in size and their surfaces have a dominating influence, high internal surface tension can then force the film volume toward compression, as observed at the highest pressures in Figure 3.

For optimal CIGS device performance, the desirable Mo films display a fibrous morphology closer to that of the rf sputtered films that allows diffusion pathways for the migration of sodium (Na) atoms from the underlying soda lime glass (SLG) substrate to the CIGS layer during its deposition [5].

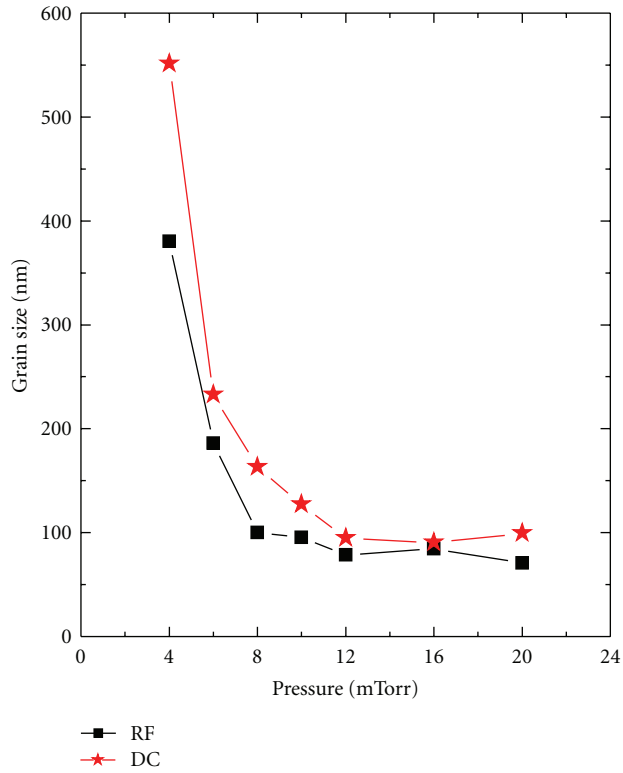

Figure 4: Variation of average grain size of rf and dc films as a function of pressure. The lines connect data points as guides to the eye.

3.2. Electrical Properties. The resistivity of the rf and dc films was found to increase with increasing pressure (Figure 6). The rf films were found to be more resistive compared to the dc films under otherwise identical deposition conditions. The higher conductivity at low pressure is consistent with a dense microstructure, whereas the low conductivity at high pressure correlates well with porous microstructure associated with tensile strain in the films. Low conductivity at higher pressure is also consistent with decreasing grain size.

3.3. Optical Properties. During the deposition of the molybdenum films, real time *in situ* spectroscopic ellipsometry (RTSE) was used over a wide spectral range (0.75–6.5 eV) in order to characterize the growth process and the dielectric functions. We chose 10 mTorr as a characteristic pressure, where high tensile strain is observed for both rf and dc films.

Figure 7 shows the surface roughness and the bulk layer thickness as a function of deposition time extracted from RTSE as the film is deposited. During the initial stage of growth, the incident Mo atoms nucleate forming separate islands which is evidenced by a sharp increase in the surface roughness thickness [22]. The Mo island size for the rf films relative to the dc films is slightly greater, as measured normal to the film surface at the onset of coalescence. Island coalescence is characterized by a subsequent decrease in surface roughness simultaneously with the onset of bulk layer growth. A linear extrapolation of the bulk growth in the uniform growth regime allows calculation of the deposition rates and the final thickness. These thicknesses are found to be in excellent agreement with *ex situ* surface profilometry measurements. After complete coalescence of the islands, the surface roughness thickness increases slightly before saturating to a value of 3.9 nm (dc films) and 5 nm (rf films) which correlates well with the *ex situ* AFM measurements of 2.9 nm and 3.8 nm. Both rf and dc sputtered Mo thin films follow a similar trend of surface roughness and bulk layer thickness variation, but smoother film morphology and higher deposition rates are obtained for the dc films compared with the rf films.

Figures 8 and 9 show the complex dielectric function components $(\varepsilon_1, \varepsilon_2)$ of the Mo films at two bulk layer thicknesses (3.3 nm and 100 nm), as determined by exact inversion of spectra collected in real time during the growth process. The bulk layer thickness used in the inversion was determined through a global fit to spectra collected over a narrow time range [23]. The surface roughness in this comparison was neglected as it was relatively thin. Clear differences in $(\varepsilon_1, \varepsilon_2)$ are observed for rf and dc films at the two thicknesses. At the beginning of the growth (3.3 nm), the overall amplitude of ε_2 for the dc films is larger, indicating less void volume fraction in the dc films. This is an indication of greater coalescence in the dc film at a given thin-layer thickness. Furthermore as the thickness increases from 3.3 nm to 100 nm, the amplitude of ε_1 at the minimum photon energy of 0.75 eV sharply decreases from 9 to -22 and from -6 to -54, for the rf and dc films respectively. This is an indication of an increase in Drude free-electron relaxation time (τ) most likely due to larger grain sizes and reduced grain boundary scattering as the films increase in thickness.

From the full set of dielectric function spectra, collected every 1.5 s during the film growth, an electronic relaxation time was extracted as a function of bulk layer thickness for rf and dc films. This was done by fitting each dielectric function to a Drude free-electron model combined with a broad Lorentz oscillator [24]. The Drude model serves to extract information from the low energy portion of the spectra while the broad Lorentz oscillator serves to represent all background contributions to the dielectric function from higher energy. The Lorentz oscillator component of the model is too broad and weak in the case of our Mo films, so no information can be reliably extracted from it. The Drude model on the other hand allows for a determination of the broadening parameter, Γ, which is inversely proportional to the free electron relaxation time, that is, $\tau \sim \hbar/\Gamma$, where $\hbar$ is Planck's constant. The Drude free-electron equation is given by:

$$\varepsilon(E) = \varepsilon_\infty - \frac{E_p^2}{E(E + i\Gamma)}, \tag{4}$$

where E_p is the free-electron plasma energy and ε_∞ is the contribution to the dielectric function due to higher energy oscillators, that is, the contribution from the interband transitions (excluding the Lorentz oscillator used to obtain a suitable fit). The resulting best-fit relaxation time (τ) as a

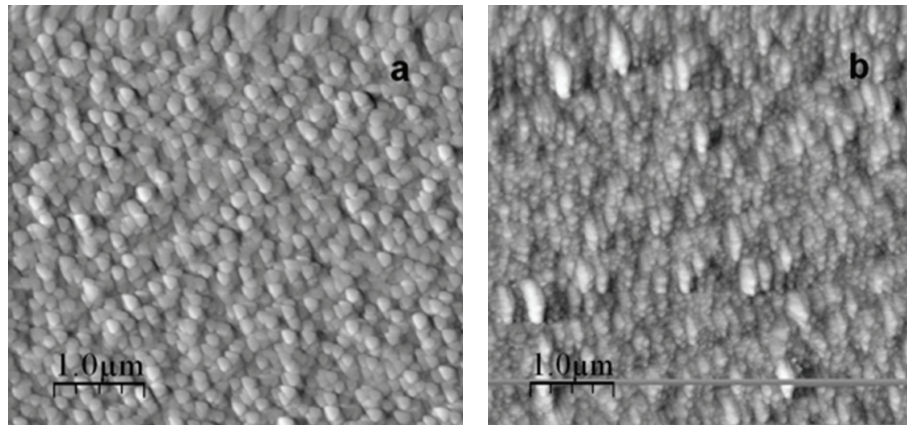

(a) (b)

Figure 5: Topographical images (5 μm × 5 μm) of dc (a) and rf (b) sputtered Mo deposited at 4 mTorr Ar pressure.

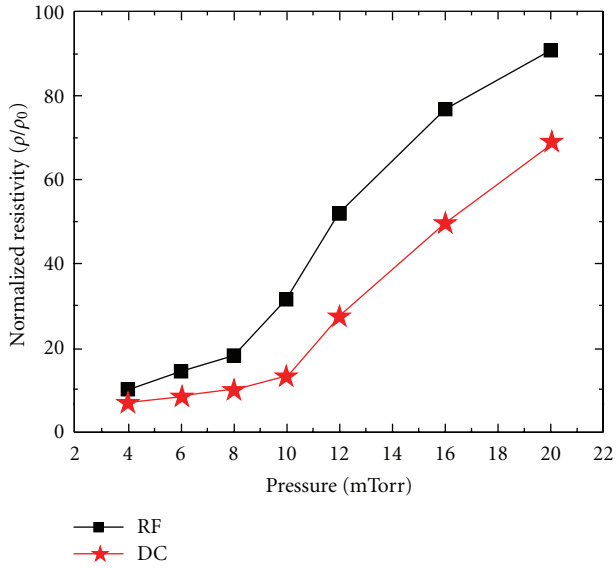

Figure 6: Normalized resistivity as a function of pressure for Mo thin films.

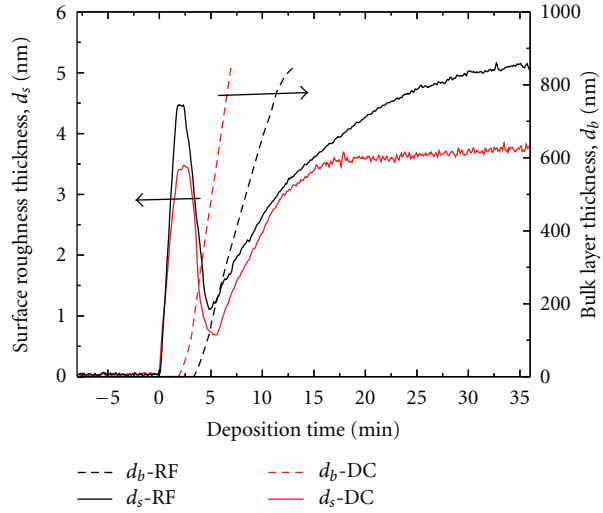

Figure 7: Evolution of surface roughness (solid line) and bulk layer thicknesses (dashed line) obtained by RTSE for Mo deposition using dc and rf sputtering at 10 mTorr. The bulk layer becomes fully opaque at large thickness values and, as a result, its thickness cannot be determined.

function of bulk layer thickness, d_b, is shown in Figure 10. It shows that both rf and dc films have a similar trend for τ, that is, initial increase with increase in d_b and saturation toward the end, most likely when the grain grows with diameter comparable to the bulk thickness. It is important to note that the relaxation time for the rf films is systematically lower than that for the dc films.

The particular functional electronic relaxation time observed in Figure 10 can be attributed to grain boundary scattering. To model this behavior, we use the model proposed by Kasap [25], following (5):

$$\tau^{-1} = \tau_b^{-1} + \frac{3\Re\nu_F}{\left[2(1-\Re)\lambda_g\right]}, \tag{5}$$

where τ_b is the relaxation time in the limit of a single crystal, $\nu_F = 1.7 \times 10^6$ m/s is the Fermi velocity for Mo, λ_g is the electron mean free path, and $\Re$ is the grain boundary reflection coefficient, taken to be 0.5 as a first approximation [15]. Reasonable fits to the data for τ in Figure 10 are obtained if one assumes that the mean free path λ_g is proportional to the grain radius and that the crystallite evolution follows a conical growth mode in accordance the relationship $\lambda_g = xd_b$. Values of $x = 0.33$ (rf films) and $x = 0.45$ (dc films) were extracted. This higher value of the grain size for the dc films compared to the rf films is consistent with the XRD results.

4. Conclusion

Molybdenum thin films were deposited onto soda-lime glass substrates, using rf and dc magnetron sputtering. We have

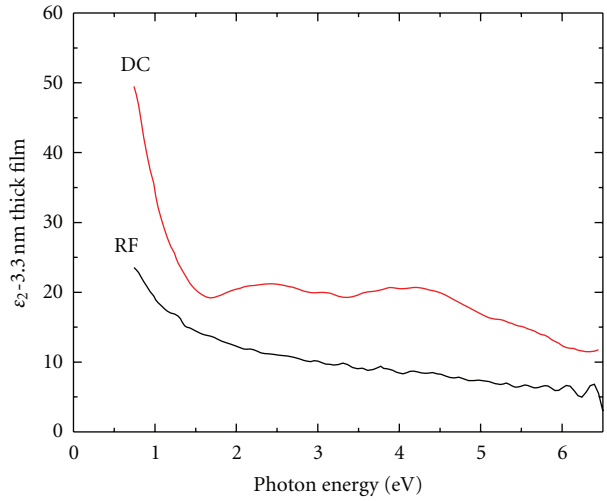

Figure 8: A comparison of the imaginary parts of the dielectric function for 3.3 nm thick Mo films deposited by rf and dc sputtering at 10 mTorr.

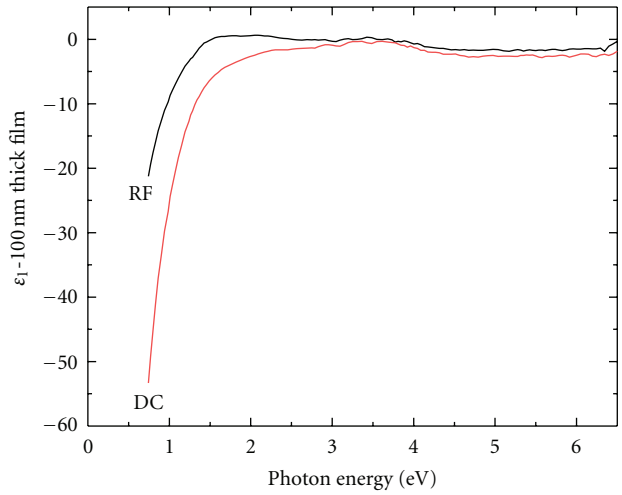

Figure 9: A comparison of the real parts of the dielectric function for 100 nm thick Mo films deposited by rf and dc sputtering at 10 mTorr.

shown that critical sputtering parameters which control the mechanisms and kinetics of film growth are not only pressure and power but also the deposition mode (rf versus dc). Both rf and dc deposited films show similar trends in microstructural evolution, characterized by a Volmer-Weber island growth-coalescence process followed by a continuous increase of the grain size according to a cone-growth model. The strain in the film also varied similarly for both films, transitioning from compressive through tensile and back to compressive again. Interestingly, this has little effect on the adhesion of the films, which was good for all films except those deposited by dc sputtering at low pressure. It is important to note, however, that these films have not been exposed to the CIGS deposition process at 550°C under Se atmosphere, and therefore could still delaminate during solar cell fabrication. Another parameter to take into

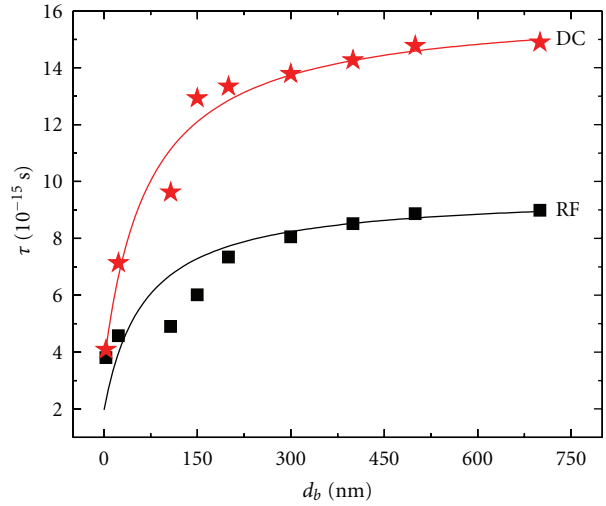

Figure 10: Relaxation time τ for free electrons in Mo as a function of the bulk layer thickness for both dc and rf mode sputtering. Also shown are the results of fits using a simple conical grain growth model.

account, depending on the CIGS deposition process, is the ability of the molybdenum to serve as a conduit for sodium diffusion from the glass. Here, our experiments have shown that the dc films have larger grains from the beginning to the end of the growth, which may be less advantageous for sodium diffusion through grain boundaries. Finally, the lower conductivity of the rf films can be seen as a problem since this may increase the solar cell series resistance. The lower conductivity may also be an indicator of the presence of foreign atoms (such as oxygen), which in turn may allow for more flexibility of the film and less delamination when deposition is performed on flexible substrates [26].

References

[1] P. Jackson, D. Hariskos, E. Lotter et al., "New world record efficiency for Cu(In,Ga)Se_2 thin-film solar cells beyond 20%," *Progress in Photovoltaics: Research and Applications*, vol. 19, no. 7, pp. 894–897, 2011.

[2] K. Orgassa, H. W. Schock, and J. H. Werner, "Alternative back contact materials for thin film Cu(In,Ga)Se_2 solar cells," *Thin Solid Films*, vol. 431-432, pp. 387–391, 2003.

[3] J. H. Scofield, A. Duda, D. Albin, B. L. Ballard, and P. K. Predecki, "Sputtered molybdenum bilayer back contact for copper indium diselenide-based polycrystalline thin-film solar cells," *Thin Solid Films*, vol. 260, no. 1, pp. 26–31, 1995.

[4] A. A. Kadam, A. H. Jahagirdar, and N. G. Dhere, "Effect of stresses in molybdenum back contact film on properties of CIGSS absorber layer," in *Proceedings of the Materials Research Society Spring Meeting*, pp. 423–429, April 2005.

[5] H. A. Al-Thani, F. S. Hasoon, M. Young et al., "The effect of Mo back contact on Na out-diffusion and device performance of Mo/Cu(In,Ga)Se_2/CdS/ZnO solar cells," in *Proceedings of the 29th IEEE Photovoltaic Specialists Conference*, pp. 720–723, New Orleans, La, USA, May 2002.

[6] G. Gordillo, M. Grizález, and L. C. Hernandez, "Structural and electrical properties of DC sputtered molybdenum films,"

Solar Energy Materials and Solar Cells, vol. 51, no. 3-4, pp. 327–337, 1998.

[7] M. C. K. Tinone, T. Haga, and H. Kinoshita, "Multilayer sputter deposition stress control," *Journal of Electron Spectroscopy and Related Phenomena*, vol. 80, pp. 461–464, 1996.

[8] L. Assmann, J. C. Bernède, A. Drici, C. Amory, E. Halgand, and M. Morsli, "Study of the Mo thin films and Mo/CIGS interface properties," *Applied Surface Science*, vol. 246, no. 1–3, pp. 159–166, 2005.

[9] N. Miyata and S. Akiyoshi, "Preparation and electrochromic properties of rf-sputtered molybdenum oxide films," *Journal of Applied Physics*, vol. 58, no. 4, pp. 1651–1655, 1985.

[10] M. A. Martínez and C. Guillén, "Effect of r.f.-sputtered Mo substrate on the microstructure of electrodeposited $CuInSe_2$ thin films," *Surface and Coatings Technology*, vol. 110, no. 1-2, pp. 62–67, 1998.

[11] C. Dicov, M. Marinov, H. Maciel, K. Grigorov, I. Nedkov, and G. Beshkov, "Properties of Cr and Mo thin films deposited by RF sputtering," *Journal of Optoelectronics and Advanced Materials*, vol. 7, no. 1, pp. 385–387, 2005.

[12] T. Wada, "Microstructural characterization of high-efficiency $Cu(In,Ga)Se_2$ solar cells," *Solar Energy Materials and Solar Cells*, vol. 49, no. 1–4, pp. 249–260, 1997.

[13] J. Nagano, "Electrical resistivity of sputtered molybdenum films," *Thin Solid Films*, vol. 67, no. 1, pp. 1–8, 1980.

[14] H. Khatri and S. Marsillac, "The effect of deposition parameters on radiofrequency sputtered molybdenum thin films," *Journal of Physics Condensed Matter*, vol. 20, no. 5, Article ID 055206, 2008.

[15] S. Marsillac, N. Barreau, H. Khatri et al., "Spectroscopic ellipsometry studies of In_2S_3 top window and Mo back contacts in chalcopyrite photovoltaics technology," *Physica Status Solidi C*, vol. 5, no. 5, pp. 1244–1248, 2008.

[16] J. D. Walker, H. Khatri, V. Ranjan, J. Li, R. W. Collins, and S. Marsillac, "Electronic and structural properties of molybdenum thin films as determined by real-time spectroscopic ellipsometry," *Applied Physics Letters*, vol. 94, no. 14, Article ID 141908, 2009.

[17] J. Lee, P. I. Rovira, I. An, and R. W. Collins, "Rotating-compensator multichannel ellipsometry: applications for real time Stokes vector spectroscopy of thin film growth," *Review of Scientific Instruments*, vol. 69, no. 4, pp. 1800–1810, 1998.

[18] B. Johs, J.A. Woollam, C.M. Herzinger, J.N. Hilfiker, R. Synowicki, and C. Bungay, "Overview of variable angle spectroscopic ellipsometry (VASE), Part II: advanced applications," in *Proceedings of the Society of Photo-Optical Instrumentation Engineers*, vol. 72, pp. 29–58, 1999.

[19] H. Windischmann, "Intrinsic stress in sputter-deposited thin films," *Critical Reviews in Solid State and Materials Sciences*, vol. 17, no. 6, pp. 547–596, 1992.

[20] T. Yamaguchi and R. Miyagawa, "Effects of oxygen on the properties of sputtered molybdenum thin films," *Japanese Journal of Applied Physics, Part 1*, vol. 30, no. 9, pp. 2069–2073, 1991.

[21] N. Kasai and M. Kakudo, "Springer series in chemical physics: preface," *Springer Series in Chemical Physics*, vol. 80, pp. 364–365, 2005.

[22] H. V. Nguyen, I. An, and R. W. Collins, "Evolution of the optical functions of thin-film aluminum: a real-time spectroscopic ellipsometry study," *Physical Review B*, vol. 47, no. 7, pp. 3947–3965, 1993.

[23] I. An, Y. M. Li, C. R. Wronski, H. V. Nguyen, and R. W. Collins, "*In situ* determination of dielectric functions and optical gap of ultrathin amorphous silicon by real time spectroscopic ellipsometry," *Applied Physics Letters*, vol. 59, no. 20, pp. 2543–2545, 1991.

[24] F. Wooten, *Optical Properties of Solids*, chapter 3, Academic Press, San Diego, Calif, USA, 1972.

[25] S. O. Kasap, *Principles of Electronic Materials and Devices*, McGraw Hill, New York, NY, USA, 3rd edition, 2006.

[26] E. Eser, S. Fields, G. Hanket, R. W. Birkmire, and J. Doody, "Critical issues in vapor deposition of $Cu(InGa)Se_2$ on polymer web: source spitting and back contact cracking," in *Proceedings of the 31st IEEE Photovoltaic Specialists Conference*, pp. 515–518, January 2005.